Competition within low-density bacterial populations as an unexpected factor regulating carbon decomposition in bulk soil

Alexandre Coche[a*], Tristan Babey[b], Alain Rapaport[c], Laure Vieublé Gonod[d], Patricia Garnier[d], Naoise Nunan[e,f], Jean-Raynald de Dreuzy[a]

[a] Univ Rennes, CNRS, Géosciences Rennes - UMR 6118, F-35000 Rennes, France

[b] Stanford University, Department of Earth System Science, Stanford, USA

[c] MISTEA, Univ. Montpellier, INRAE, Montpellier SupAgro, France

[d] UMR Ecosys, INRAE, AgroParisTech, Université Paris-Saclay, 78850, Thiverval Grignon, France

[e] Sorbonne Université, CNRS, IRD, INRAE, P7, UPEC, Institute of Ecology and Environmental Sciences—Paris, 4 place Jussieu, 75005 Paris, France

[f] Department of Soil & Environment, Swedish University of Agricultural Sciences, P.O. Box 7014, 75007 Uppsala, Sweden

[*] Corresponding author. *E-mail address*: alexandre.co@hotmail.fr (A. Coche)

Abstract

Bacterial decomposition of organic matter in soils is generally believed to be mainly controlled by the access bacteria have to their substrate. The influence of bacterial traits on this control has, however, received little attention. Here, we develop a bioreactive transport model to screen the interactive impacts of dispersion and bacterial traits on mineralization. We compare the model results with two sets of previously performed cm-scale soil-core experiments in which the mineralization of the pesticide 2,4-D was measured under well-controlled initial distributions and transport conditions. Bacterial dispersion away

from the initial substrate location induced a significant increase in 2,4-D mineralization, revealing the existence of a regulation of mineralization by the bacterial decomposer density, in addition to the dilution of substrate. This regulation of degradation by density becomes dominant for bacteria with an efficient uptake of substrate at low substrate concentrations (a common feature of oligotrophs). The model output suggests that the distance between bacteria adapted to oligotrophic environments is a stronger regulator of degradation than the distance between these bacteria and the substrate initial location. Such oligotrophs, commonly found in soils, compete with each other for substrate even at remarkably low population densities. The ratio-dependent Contois growth model, which includes a density regulation in the expression of the uptake efficiency, provide a more versatile representation than the substrate-dependent Monod model in these conditions. In view of their strong interactions, bioreactive and transport processes cannot be handled independently but should be integrated, in particular when reactive processes of interest are carried out by oligotrophs.

Keywords: biodegradation of organic matter; heterogeneous spatial distributions; bioreactive transport model; competition for substrate; bacterial traits; ratio-dependent growth

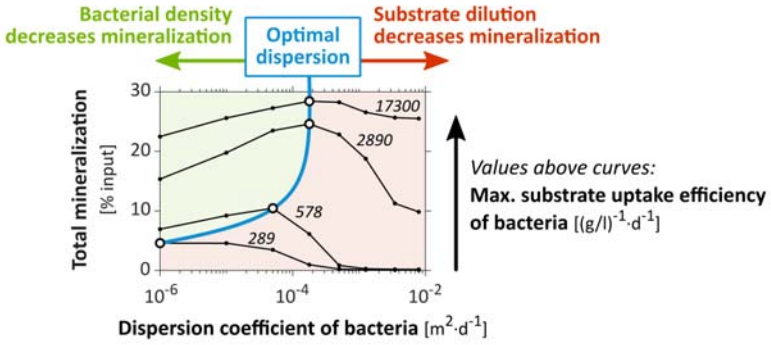

Highlights

- The impact of spatial distributions on decomposition depends on bacterial traits
- Decomposition can be reduced by competition between bacteria even at low densities

- Bacterial density regulation counterbalances substrate accessibility regulation
- Regulation of decomposition by bacterial density is more acute for oligotrophs

1. Introduction

Organic carbon is involved in most ecological functions provided by soils (Bünemann et al., 2018). Its cycling in soil depends upon the activity of microorganisms. Soluble organic molecules are taken up as substrates by specific populations of soil bacteria, and degraded inside the cells by endoenzymes to provide carbon and energy. This is precisely the case for the 2,4-Dichlorophenoxyacetic acid (2,4-D) used in this study as a generic model compound (Don and Weightman, 1985; Pieper et al., 1988; Boivin et al., 2005). Bacterial degradation of soil carbon has generally been modeled with the Monod equation, where the specific substrate uptake rate is controlled by substrate concentration and bacterial traits such as the maximum specific growth rate, the yield (or carbon use efficiency) and the "maximum uptake efficiency" (e.g. Monod, 1949; Sinton et al., 1986; Cheyns et al., 2010). With the Monod equation, at the lowest substrate concentration, the specific uptake rate is linearly proportional to the substrate concentration. The proportionality factor is referred to here as the "maximum uptake efficiency" and it reflects the maximal ability of the cell to capture substrate molecules that collide with its membrane (Button, 1978, 1983). The maximum uptake efficiency can also be understood as the volume from which a cell can harvest substrate per unit of time, as used in some studies (Desmond-Le Quéméner and Bouchez, 2014; Nunan et al., 2020; Ugalde-Salas et al., 2020). Each bacterium is assumed to be exposed to the whole substrate concentration of its surroundings, without any limitation by the population density (Lobry and Harmand, 2006).

The direct contact (exposure) between bacteria and substrate depends on their spatial distributions (Holden and Firestone, 1997; Nunan et al., 2007). Bacteria and substrate are both heterogeneously distributed as a result of numerous biotic and abiotic processes (Dechesne et al., 2014; Kuzyakov and

62 Blagodatskaya, 2015). There are complex feedback loops between these distributions, dispersive transport
63 processes such as diffusion and hydrodynamic dispersion (Madsen and Alexander, 1982; Breitenbeck et al.,
64 1988), and the bacterial activity itself such as consumption and growth (Poll et al., 2006).

65 Aggregated bacterial distributions, as observed at mm-scale for 2,4-D degraders (Vieublé Gonod et al.,
66 2003), have been shown to decrease degradation rates when the distribution of substrate is homogeneous
67 (Pallud et al., 2004; Dechesne et al., 2010). Yet, the role of bacterial metabolic traits on the impact of
68 bacterial and substrate distributions on degradation remains mostly unknown, especially when substrate
69 and bacteria are heterogeneously and dynamically redistributed in soils over µm-to-cm scales by numerous
70 spatial disturbances (Madsen and Alexander, 1982; Breitenbeck et al., 1988; König et al., 2020). We
71 investigated the extent to which bacterial activity and transport processes can be treated independently or
72 should be integrated to characterize, understand and predict degradation under various advective,
73 diffusive and dispersive conditions. The simultaneous characterization of the impacts of bacterial traits and
74 transport parameters through their mutual interactions is methodologically challenging. It requires several
75 well-controlled experiments in comparable degradation conditions, with specific spatial distributions of
76 substrate and degraders in specific transport conditions, and a spatiotemporal monitoring of the different
77 carbon pools.

78 Among the scarce relevant datasets (e.g. Dechesne et al., 2010), we used the two sets of cm-scale soil-core
79 experiments performed by Pinheiro et al. (2015, 2018), in which the degradation of 2,4-D under different
80 initial spatial distributions and transport conditions was measured in similar repacked soil columns. Mostly
81 reported independently, they have shown first that the proximity between bacteria and the initial location
82 of a heterogeneously distributed substrate exerts a strong control on mineralization. Mineralization was
83 greater when bacteria were close to the initial location of substrate, even though most of the initial soluble
84 substrate diffused away from its initial location. This was attributed to the fact that bacteria located far
85 from the initial substrate location were only exposed to highly diluted substrate concentrations (Babey et

al., 2017). However, the hydrodynamic dispersion of both bacteria and substrate away from their initial location caused a greater than four-fold increase in the mineralization of substrate that was not leached out, to the point that it almost reached the same performance as in homogeneous conditions in which there was no dilution (Pinheiro et al., 2018). The surprising increase in mineralization suggests a regulation of mineralization by population density compensating the effect of substrate dilution, the activity of bacteria being enhanced when their density is diluted by the dispersive percolation events. While such regulations by bacterial density have not yet been considered in soils, presumably because of the extremely low apparent bacterial densities found in soils (Young et al., 2008), they are well known in bioreactors, where they are usually modeled by the ratio-dependent Contois growth law (Contois, 1959; Harmand and Godon, 2007).

In order to determine the relevance of the putative bacterial decomposer density effect on decomposition, we developed a quantitative approach to model the two sets of experiments within the same unified framework (section 2). We assessed the relevance of previously developed models, improved the calibration of a Monod-based model and investigated an alternative Contois-based model (section 3). We discuss the implication of the results on the controlling factors of soil organic carbon cycling, on the relevant bacterial growth models and on the possible bacterial strategies (section 4).

2. Models and methods

2.1. Experiment scheme, geometry and initial distributions

We briefly introduce the experiments performed previously and highlight aspects of the experiments that are important for the modeling (**Fig. 1**). The full experimental setting is presented in the supplementary materials (**Fig. S1** and **Table S1**) for the sake of completeness. Soil columns were packed with two homogeneous or heterogeneous arrangements of soil cubes, either sterilized, or hosting the indigenous

L08 microbial communities (referred to as "degraders") and amended with ^{14}C-labelled 2,4-D (referred to as
L09 "substrate"). Two sets of experiments, referred to as "hydrostatic" and "percolation" conditions, were
L10 performed respectively with only substrate diffusion (Pinheiro et al., 2015), or with additional substrate
L11 and bacterial advection and dispersion caused by water percolation (Pinheiro et al., 2018). The initial
L12 locations of the bacteria and substrate were set in the model according to the experimental conditions
L13 (**Fig 1A**). Initial concentrations used in the model are detailed in **Table 1**. In the experiments, the mass of
L14 mineralized ^{14}C derived from the degradation of the labelled 2,4-D was monitored at the core scale during
L15 at least two weeks (**Fig. 1B**). These data were used to confront the model processes with a physical system,
L16 as detailed in section 2.5.

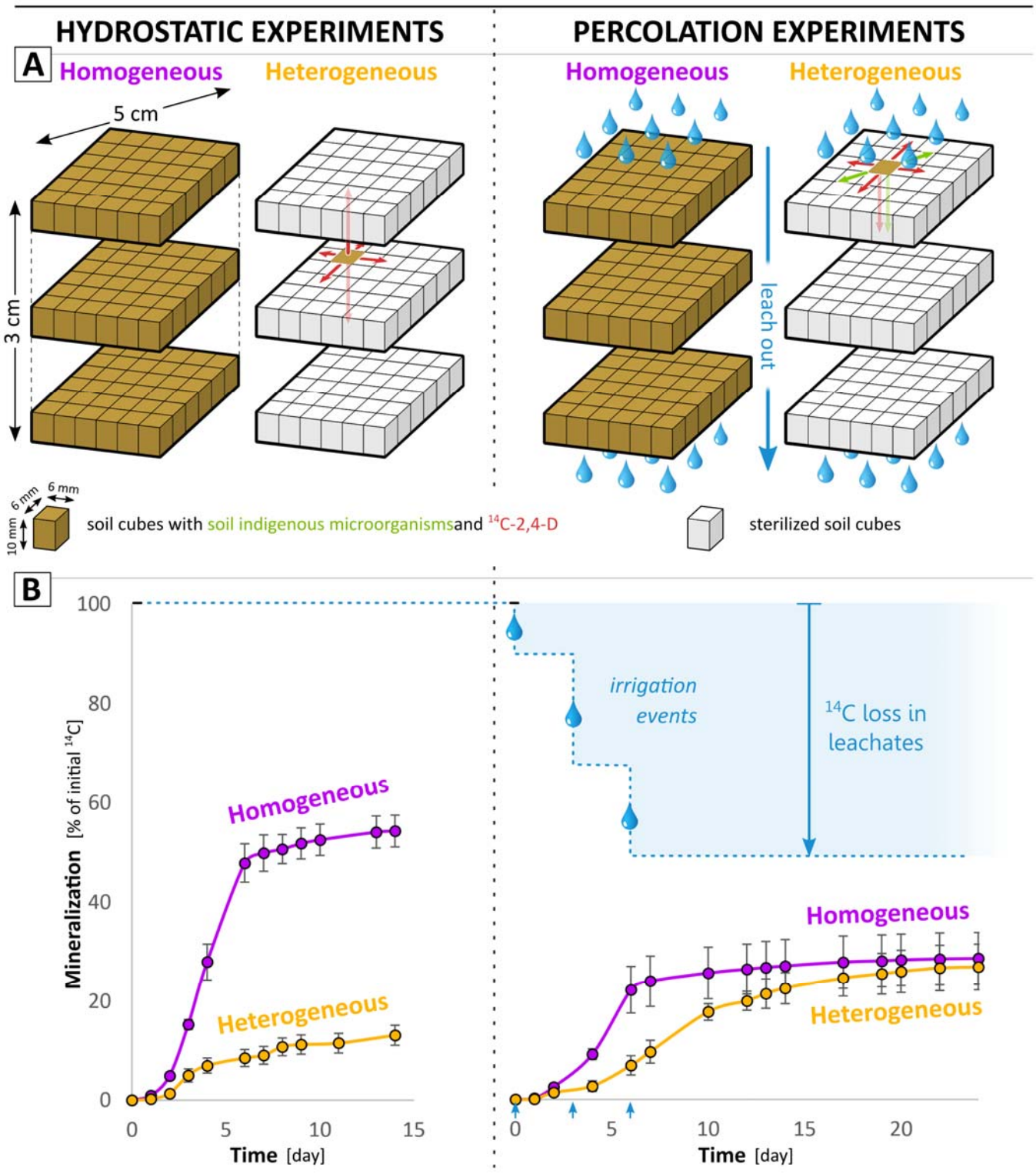

Fig. 1. Model experimental design, geometry and initial distributions (**A**) based on previously performed experiments in hydrostatic (Pinheiro et al., 2015) and percolation (Pinheiro et al., 2018) conditions. The red and green arrows refer respectively to the 2,4-D and degrader modeled displacements. (**B**) Experimental

cumulated production of CO_2 (adapted from Pinheiro et al. (2018, 2015), permission for reproduction granted by Elsevier).

2.2. Bioreactive model

The bioreactive model extends the model published by Babey et al. (2017) (**Fig. 2**) to account for Contois growth law as an alternative to Monod's. The sorption processes, the bacterial lag phase and the nutrient recycling described below were previously discussed and their use justified in Babey et al. (2017) to consistently represent the experimental data. The $r(\cdot)$ notation expresses the reaction rates of the biochemical dynamics that are expressed as follows:

$$r(S) = k_{AS}\, A - k_{SA}\, S - k_R\, S - \frac{\mu}{y} B + m_t\, \chi\, B \quad (1)$$

$$r(A) = k_{SA}\, S - k_{AS}\, A \quad (2)$$

$$r(R_S) = k_R\, S \quad (3)$$

$$r(CO_2) = \frac{(1-y)}{y} \mu\, B \quad (4)$$

$$r(B) = \mu\, B - m_t\, B \quad (5)$$

$$r(R_B) = m_t(1-\chi)B \quad (6)$$

All variable and parameter definitions are listed in **Table 1**. The dynamics of the specific growth rate μ are given, for the Monod-based model, by:

$$\frac{\partial \mu}{\partial t} = \alpha \left(\mu_{max} \frac{S}{\kappa_M + S} - \mu \right) \quad (7)$$

and, for the Contois-based model, by:

$$\frac{\partial \mu}{\partial t} = \alpha \left(\mu_{max} \frac{S/B}{\kappa_C + S/B} - \mu \right) = \alpha \left(\mu_{max} \frac{S}{\kappa_C B + S} - \mu \right) \quad (8)$$

where $\mu = 0$ at $t = 0$.

The soluble substrate S is either reversibly adsorbed to soil particles (pool A) or irreversibly adsorbed (pool R_S) (Eqs. (1), (2), (3)), or taken up by bacteria B (Eq. (1)) and metabolized into CO_2 (Eq. (4)) and new biomass B (Eq. (5)). k_{SA} and k_{AS} are the reversible sorption coefficients. k_R is the irreversible one. Bacteria death occurs at a constant rate m_t (Eq. (5)) and a fraction of the bacterial necromass is considered to return to the soluble substrate pool S to account for nutrient recycling (Eq. (1)), while the rest is transformed to biotic residues R_B (Eq. (6)). The nutrient recycling is necessary to adequately predict the late dynamics of mineralization. Its impact on mineralization is only marginal during the first five days. The adsorbed substrate and biotic residues form the pool of insoluble carbon $A + R_S + R_B$. The substrate S is consumed by bacteria B according to their specific uptake rate $(1/y)\cdot\mu$ expressed either by the substrate-dependent Monod growth law (Eq. (7)) (Monod, 1949) or by the ratio-dependent Contois growth law (Eq. (8)) (Contois, 1959). y is the yield coefficient and relates the specific uptake rate $(1/y)\cdot\mu$ to the specific growth rate μ. μ_{max} is the maximum specific growth rate. κ_M and κ_C are Monod and Contois constants respectively. The effective uptake is delayed by the accommodation rate α, which explicitly takes into account the "memory" effects of the bacteria when adapting to new conditions (Patarinska et al., 2000). This delay is necessary to capture the mineralization lag time at the beginning of the experiments (see **Fig. S6**). Over long time periods ($t \gg 1/\alpha$), μ follows the exact expression of the Monod or Contois equations. All modeled pools (S, B, CO_2, A, R_S and R_B) were expressed as carbon concentrations in $\mu g \cdot g^{-1}$ (mass of carbon per mass of dry soil) considering a soil water content of 0.205 $g \cdot g^{-1}$ (mass of water per mass of dry soil), a bulk density of the soil column of 1.3 10^3 $g \cdot l^{-1}$ (mass of dry soil per apparent soil volume) and an average bacterial dry weight of 2.8 10^{-13} g corresponding to 1.49 10^{-13} g of carbon per cell. These values of water content and bulk density were those set up in the experiments, the latter corresponding to a water potential adjusted at -31.6 kPa (pF 2.5). The average bacterial weight was assumed based on Dechesne et al. (2010) and Pinheiro et al. (2015). The water-filled pore space (54%, volume of water per volume of pores) was such that oxygen was not considered a limiting factor for 2,4-D degradation.

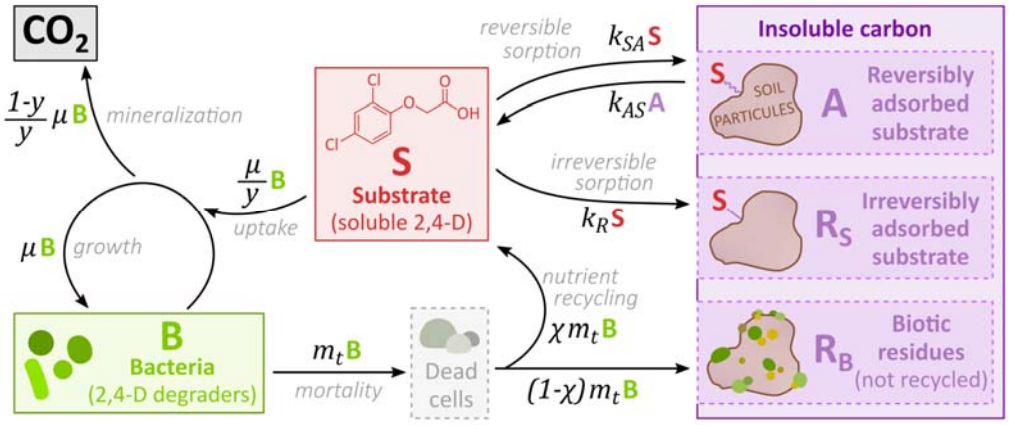

Fig. 2. Graphical representation of the biochemical model and carbon fluxes identified by the arrows. Under low substrate concentrations S, the specific uptake rate $(1/y)\cdot\mu$ becomes equal to $S\cdot(1/y)\cdot\mu_{max}/\kappa_M$, where $(1/y)\cdot\mu_{max}/\kappa_M$ is referred to as the "maximum uptake efficiency".

2.3. Reactive transport model

The transport model is based on the diffusion model of Babey et al. (2017) to which advective-dispersive processes explored in the experiments of Pinheiro et al. (2018) are added. Bacterial leaching out and dispersion were observed only in the percolation experiments while the substrate was also reported to diffuse. Hydrodynamic leaching and dispersion were modeled independently, as they result from, respectively, bypass flow through large pores and complex hydrodynamic dispersion processes coming not only from usual flow mechanisms but also from large saturation variations and local redistribution of moisture in the pore network. Due to the lack of adequate experimental data to characterize the details of the dispersion process, we applied a simple isotropic dispersion coefficient. Complementary numerical simulations show that other anisotropic dispersion parameterization are only weakly sensitive (**Fig. S3**). Bacterial and substrate transports were described with the same advective and dispersive parameters. This assumption did not significantly alter the results (**Fig. S4**). Coupled to the equations of the bioreactive model ((1)-(8)), the full reactive transport model is given by:

$$\frac{\partial S}{\partial t} = r(S) + \nabla\left(d_{diff}\nabla S\right) + G\left(\nabla\left(d_{disp}\nabla S\right) - \nu S\right) \quad (9)$$

$$\frac{\partial B}{\partial t} = r(B) + G\left(\nabla\left(d_{disp}\nabla B\right) - \nu B\right) \quad (10)$$

$$\frac{\partial U}{\partial t} = r(U) \qquad \text{for } U = A, R_B, R_S \text{ and } CO_2 \quad (11)$$

where d_{diff} is the effective molecular diffusion coefficient of S, d_{disp} is the effective hydrodynamic dispersion coefficient of S and B and ν is their leaching rate. Note that the dispersion coefficient d_{disp} mostly affected the spreading of bacteria, given that substrate was mainly spread by diffusion, as noted in section 2.3 and confirmed by consistent results from equivalent models without hydrodynamic dispersion of S (**Fig. S5**). Effective diffusion and dispersion processes were assumed to be isotropic and uniform at the column-scale. Dispersion and leaching were active only during the observed 1-hour percolation events at days 0, 3 and 6 as controlled by the function G defined as:

$$G(t) = 1 \quad t = [0\text{d} - 0\text{d}1\text{h}]; [3\text{d} - 3\text{d}1\text{h}]; [6\text{d} - 6\text{d}1\text{h}]$$
$$G(t) = 0 \quad \text{otherwise.} \quad (12)$$

No-flow boundary conditions were imposed at the edges of the soil core ($\nabla S = 0$ and $\nabla B = 0$) during periods outside of the percolation events. The transient evolutions of the water content and their effects on concentrations were not considered because of the short duration of the percolation events (1 h) and the absence of detectable effects on the experimental mineralization curve around the percolation events (**Fig. 1D**). Hydration conditions were considered constant, constrained by the water potential adjusted to -31.6 kPa. No bacterial mobility was observed in the hydrostatic experiments, suggesting that the bacterial mobility observed in the percolation experiments resulted primarily from hydrodynamic dispersion.

Carbon pools concentration dynamics were simulated on a 3 × 6 × 6 regular mesh grid. Although the shape of the grid was slightly different from that of the cylindrical soil-core, it did not have any observable impact

(Babey et al., 2017). We recall that substrate and bacteria were initially co-located in the same cube(s). Each cube was considered to be physically, chemically and biologically homogeneous. Diffusion and dispersion were simulated using a finite-difference scheme (Iserles, 2009) and coupled with the bioreactive model, itself solved by the 4th order Runge-Kutta integration method function of MATLAB (Shampine and Reichelt, 1997). The coupling of transport and bioreactive models was achieved with a sequential non-iterative operator-splitting method, in which the equations are resolved within each time step in a sequence of one transport step followed by one bioreactive step (Carrayrou et al., 2004; Lagneau and van der Lee, 2010). The time steps were smaller than the characteristic diffusion and reaction times to avoid any coupling issues.

2.4. Exploratory screening

Parameters and their values are listed in **Table 1**. Sorption parameters and the diffusion coefficient were set at values that were calibrated and validated by Babey et al. (2017) in independent experiments without degradation. The mortality rate and the nutrient recycling yield were also kept at the values calibrated in Babey et al. (2017) as they were considered to be well constrained by the residual mineralization dynamics of the homogeneous hydrostatic experiment (**Fig. 1D**). The four biological parameters primarily involved in the biological response of bacteria to the concentration of substrate were determined to be $(1/y)\cdot\mu_{max}$, α, $B(t=0)$ and either $(1/y)\cdot\mu_{max}/\kappa_M$ for the Monod-based model or $(1/y)\cdot\mu_{max}/(B(t=0)\cdot\kappa_C)$ for the Contois-based model. Each of these four parameters were sampled over 7 logarithmically-distributed values within the theoretically and physically relevant ranges given by Babey et al. (2017), and all possible combinations of values were screened (**Table S2**). We recall that the "maximum uptake efficiency" $(1/y)\cdot\mu_{max}/\kappa_M$ characterizes the specific bacterial uptake of substrate at the lowest substrate concentration (Button, 1991), while the maximum specific uptake rate $(1/y)\cdot\mu_{max}$ characterizes the bacterial uptake at the highest substrate concentration. Note that the uptake yield y was fixed at the value calibrated by Babey et

al. (2017) with a high degree of certainty. The initial maximum uptake efficiency $(1/y)\cdot\mu_{max}/(B(t=0)\cdot\kappa_C)$ in the Contois-based model was screened in the same range as $(1/y)\cdot\mu_{max}/\kappa_M$. The accommodation rate α of the degrader response ranged from a negligible delay of few minutes (α = 934 d^{-1}) to a prolonged delay of around 10 days (α = 9.34 10^{-2} d^{-1}). $B(t=0)$ values were screened around the initial experimental measurements of the *tfdA* gene copy number, assuming that one *tfdA* sequence corresponded to one bacterium. They ranged over two orders of magnitude to account for the uncertainty of the conversion of *tfdA* copy number into alive 2,4-D degraders (Bælum et al., 2006, 2008). Bacterial density in the uptake efficiency expression will also be expressed in $g\cdot l^{-1}$ (mass of bacteria per volume of water) for a more direct comparison with the relevant literature.

The spatial distribution of bacteria observed at the end of the experiments could not be used to determine the effective dispersion coefficient d_{disp} (**Fig. S2**). While they qualitatively ascertained that bacteria spread orthogonally to the percolation direction, experimental data were not sufficiently resolved to be used quantitatively. The dispersion coefficient was thus screened over 10 values ranging from no dispersion (d_{disp} = 0) to complete instant homogenization of the soil core (d_{disp} = inf) (**Table S2**). The effective diffusion coefficient d_{diff} had been calibrated independently from percolation conditions (Pinheiro et al., 2015; Babey et al., 2017). The leaching rates ν were determined based on the experimental masses of leached ^{14}C (Pinheiro et al., 2018) (**Table 1**). Detailed values for the screened parameters are listed in **Table S2**.

Table 1. Values and range of values of the reactive transport model. The effective dispersion coefficient d_{disp} applies only to heterogeneous percolation experiments. $B(t=0)$ is the initial density of bacteria in the natural cubes. It is considered 1.6 times smaller in the percolation experiments than in the hydrostatic experiments according to the initial experimental measurements.

Parameter description	Symbol	Unit	Fixed values and admissible ranges for screening

initial substrate concentration	hydrostatic experiments	$S(t=0)$	$\mu g \cdot g^{-1}$ (mass of substrate carbon per mass of dry soil)	0.825 [b]
	percolation experiments		$\mu g \cdot g^{-1}$	6.52 [b]
reversible adsorption coefficient		k_{SA}	d^{-1}	0.09207
reversible desorption coefficient		k_{AS}	d^{-1}	4.361
irreversible adsorption coefficient		k_C	d^{-1}	0.01296
uptake yield		y	-	0.5206
maximum specific uptake rate		$(1/y)\cdot\mu_{max}$	d^{-1}	[0.0190 – 19.5]
uptake efficiency at the lowest substrate concentration		$(1/y)\cdot\mu_{max}/\kappa$ [a] *where* κ *is* κ_M *or* $B(t=0)\cdot\kappa_C$	$g \cdot \mu g^{-1} \cdot d^{-1}$ (mass of dry soil per mass of bacterial carbon per unit of time)	[0.0152 – 159] [c]
accommodation rate		α	d^{-1}	[0.00934 – 934]
initial degrader population density	hydrostatic experiments	$B(t=0)$	$\mu g \cdot g^{-1}$ (mass of bacterial carbon per mass of dry soil)	[0.0161 – 1.61] [d]
	percolation experiments	$B(t=0)$	$\mu g \cdot g^{-1}$	[0.0101 – 1.01] [d]
mortality rate		m_t	d^{-1}	0.0602
nutrient recycling yield		χ	-	0.6010
effective diffusion coefficient		d_{diff}	$m^2 \cdot d^{-1}$	$1\ 10^{-5}$ [e]
effective dispersion coefficient		d_{disp}	$m^2 \cdot d^{-1}$	[0 – ∞]
leaching rates (days 0; 3; 6)	homogeneous experiments	ν	-	0.108; 0.226; 0.180
	heterogeneous experiments			0.107; 0.223; 0.178

[a] The half-saturation constant κ corresponds to κ_M for the Monod-based model and $B(t=0)\cdot\kappa_C$ for the Contois-based model (where $B(t=0)$ is the value from the hydrostatic experiments).

[b] The initial substrate concentration $S(t=0)$ is set equal to the ^{14}C-2,4-D concentration amended in the experiments.

[c] The values of $(1/y)\cdot\mu_{max}/\kappa$ correspond to ranges of [1.65 – 1.73 10^{4}] l·g^{-1}·d^{-1} (volume of water per mass of bacteria per unit of time)

[d] The values of $B(t=0)$ correspond respectively to ranges of [1.48 10^{-4} – 1.48 10^{-2}] g·l^{-1} (mass of bacteria per volume of water) for the hydrostatic experiments and [9.24 10^{-5} – 9.24 10^{-3}] g·l^{-1} for the percolation experiments.

[e] The value of d_{diff} has been calibrated on a 3 × 6 × 6 grid in similar conditions (Babey et al., 2017).

2.5. Model to data comparison

The comparison between the results of the model and the experimental data was based on the core-scale data of mineralization deduced from the carbon mass m_{CO2} of $^{14}CO_2$ emissions:

$$m_{CO_2}(t) = \int_V CO_2(x,t)dx \qquad (13)$$

with V the volume of the soil cores. Mineralization at a given time t was expressed as the carbon mass of cumulated $^{14}CO_2$ emissions ($m_{CO_2,q}(t)$) per initial carbon mass of ^{14}C-substrate S ($m_{S,q}(t=0)$) where the index q identifies the experiment at hand. Indices *1*, *2*, *3* and *4* are respectively given to the homogeneous hydrostatic, heterogeneous hydrostatic, homogeneous percolation and heterogeneous percolation experiments. Data-to-model adequacy was assessed for each of the experiments by a classical root-mean-square evaluation function J_q comparing the modeled mineralization of Eq. (4) to the measured mineralization at the n_q available sampling times t_i:

$$J_q = \left(\frac{1}{n_q} \sum_{i=1}^{n_q} \left(\frac{m_{CO_2,q}^{mod}(t_i) - m_{CO_2,q}^{data}(t_i)}{m_{S,q}(\mathrm{t}=0)} \right)^2 \right)^{\frac{1}{2}} \quad (14)$$

Discrepancies over the full set of experiments J_{1234} were thus expressed as:

$$J_{1234} = \left(\frac{1}{4} \sum_{k=1}^{4} J_k^2 \right)^{\frac{1}{2}} \quad (15)$$

Following the systematic parameter screening described in section 2.5, the parameter set minimizing J_{1234} was determined and referred to as the set calibrated on both hydrostatic and percolation experiments. The measurement errors were in average 1.7 times higher in the percolation experiments than in the hydrostatic experiments. This was assumed to be due to differences in experimental setup between the two sets of experiments of Pinheiro et al. (2015, 2018). This error difference contributed to limit the weight of the percolation experiments when determining the best-fitting parameter set over the whole set of experiments (J_{1234}). We made the choice to give an equal weight to all experiments by only taking into account the average CO_2 values.

3. Results

3.1. Model calibration

The calibration of the bioreactive transport model carried out using only the hydrostatic experimental data (Babey et al., 2017) led to a minimal discrepancy between data and model of J_{12} = 0.023 (**Fig. 3-A1** and **A2**). This pre-existing parameterization was used to provide blind predictions of the percolation experiments, with the effective dispersion coefficient d_{disp} as an additional fitting parameter. It gave a reasonable prediction of mineralization in the homogeneous percolation experiment (J_3 = 0.038, **Fig. 3-A3**) but failed in the heterogeneous percolation experiment (J_4 = 0.151, **Fig. 3-A4**), regardless of the dispersion coefficient values. The smallest discrepancy J_4 was surprisingly obtained without any bacterial dispersion (d_{disp} = 0) in

contradiction with the bacterial spread observed in the experimental data (**Fig. S2**). The final predicted mineralization was highest when bacteria remained aggregated close to the initial location of the substrate. The highest predicted mineralization was however four times lower than the experimental data. The large gap between the experimental data and the modeled scenario suggests that bacterial proximity to the initial substrate location is not the underlying explanatory mechanism for the high mineralization rates. On the contrary, it suggests that mineralization might rather be increased by the dispersion of bacteria towards more diluted substrate concentrations, and that the identified bacterial traits do not match this increase of mineralization with dispersion.

In order to investigate the capacity of the reactive transport model to fit both hydrostatic and percolation experimental data, the biological parameters ($(1/y)\cdot\mu_{max}/\kappa_M$, $(1/y)\cdot\mu_{max}$, α, $B(t=0)$) and the dispersion coefficient (d_{disp}) were calibrated on both hydrostatic and percolation experiments following the screening approach given in section 2.4 to minimize J_{1234}. The mineralization dynamics were adequately predicted in all four experiments with the biological parameter set giving the lowest overall discrepancy (J_{1234} = 0.032) and a non-zero dispersion coefficient (d_{disp} = 1.78 10^{-4} $m^2 \cdot d^{-1}$) (**Fig. 3**, **Table 2**). The non-zero dispersion coefficient indicates that the calibrated model accounts for a positive impact of bacterial dispersion on degradation. The model results suggest that this effect is necessary to successfully predict the high degree of degradation in the experimental data. Compared to the parameters calibrated only using the hydrostatic experiments, the parameter set calibrated on both hydrostatic and percolation experiments also displayed a much higher maximum uptake efficiency $(1/y)\cdot\mu_{max}/\kappa_M$ = 26.5 $g \cdot \mu g^{-1} \cdot d^{-1}$ (mass of dry soil per mass of bacterial carbon per unit of time) (**Table 2**). The systematic exploration of the parameter space showed that high maximum uptake efficiency was a common feature of the 1% best-fitting parameterizations over both hydrostatic and percolation experiments (smallest J_{1234}), with values of 159 and 26.5 $g \cdot \mu g^{-1} \cdot d^{-1}$, corresponding respectively to 1.73 10^4 and 2.89 10^3 $l \cdot g^{-1} \cdot d^{-1}$ (volume of water per mass of bacteria per unit

295 of time). It underlines the essential role of the maximum uptake efficiency for modulating the impact of
296 dispersion on degradation, further detailed and explained in section 3.2.3.

297 **Table 2**. Parameters for the Monod-based model calibrated by the screening approach (section 2.4) on the
298 hydrostatic experiments only (Babey et al., 2017) and on both hydrostatic and percolation experiments,
299 and for the Contois-based model calibrated on both hydrostatic and percolation experiments.

Parameter symbol		Unit	Monod model calibration		Contois model calibration
			on the sole hydrostatic experiments	on both hydrostatic & percolation experiments	on both hydrostatic & percolation experiments
$(1/y)\cdot\mu_{max}$		d^{-1}	1.22	9.73	4.86
$(1/y)\cdot\mu_{max}/\kappa$ [a]		$g\cdot\mu g^{-1}\cdot d^{-1}$ (mass of dry soil per mass of bacterial carbon per unit of time)	2.65 [b]	26.5 [b]	2.65 [b]
α		d^{-1}	$9.341\ 10^{-1}$	$9.34\ 10^{-2}$	$9.34\ 10^{-2}$
$B(t=0)$	hydrostatic experiments	$\mu g\cdot g^{-1}$ (mass of bacterial carbon per mass of dry soil)	$1.61\ 10^{-1}$	$3.23\ 10^{-2}$	$3.76\ 10^{-1}$
	percolation experiments	$\mu g\cdot g^{-1}$	$1.01\ 10^{-1}$	$2.01\ 10^{-2}$	$2.34\ 10^{-1}$
d_{disp}		$m^2\cdot d^{-1}$	0 [c]	$1.78\ 10^{-4}$ [c]	10^{-5} [c]
J_{1234}		-	0.079	0.032	0.022

300 [a] The half-saturation constant κ corresponds to κ_M for the Monod-based model and $B(t=0)\cdot\kappa_C$ for the
301 Contois-based model (where $B(t=0)$ is the value from the hydrostatic experiments).

302 [b] Values of $(1/y)\cdot\mu_{max}/\kappa$ correspond respectively to $2.89\ 10^2$, $2.89\ 10^3$ and $2.89\ 10^2$ $l\cdot g^{-1}\cdot d^{-1}$ (volume of
303 water per mass of bacteria per unit of time).

[c] The corresponding spreading values induced by the hydrodynamic dispersion (root-mean-square displacements) for each percolation events are respectively 0, 3.8 and 0.91 mm, to be compared to the 25 mm radius of the soil column.

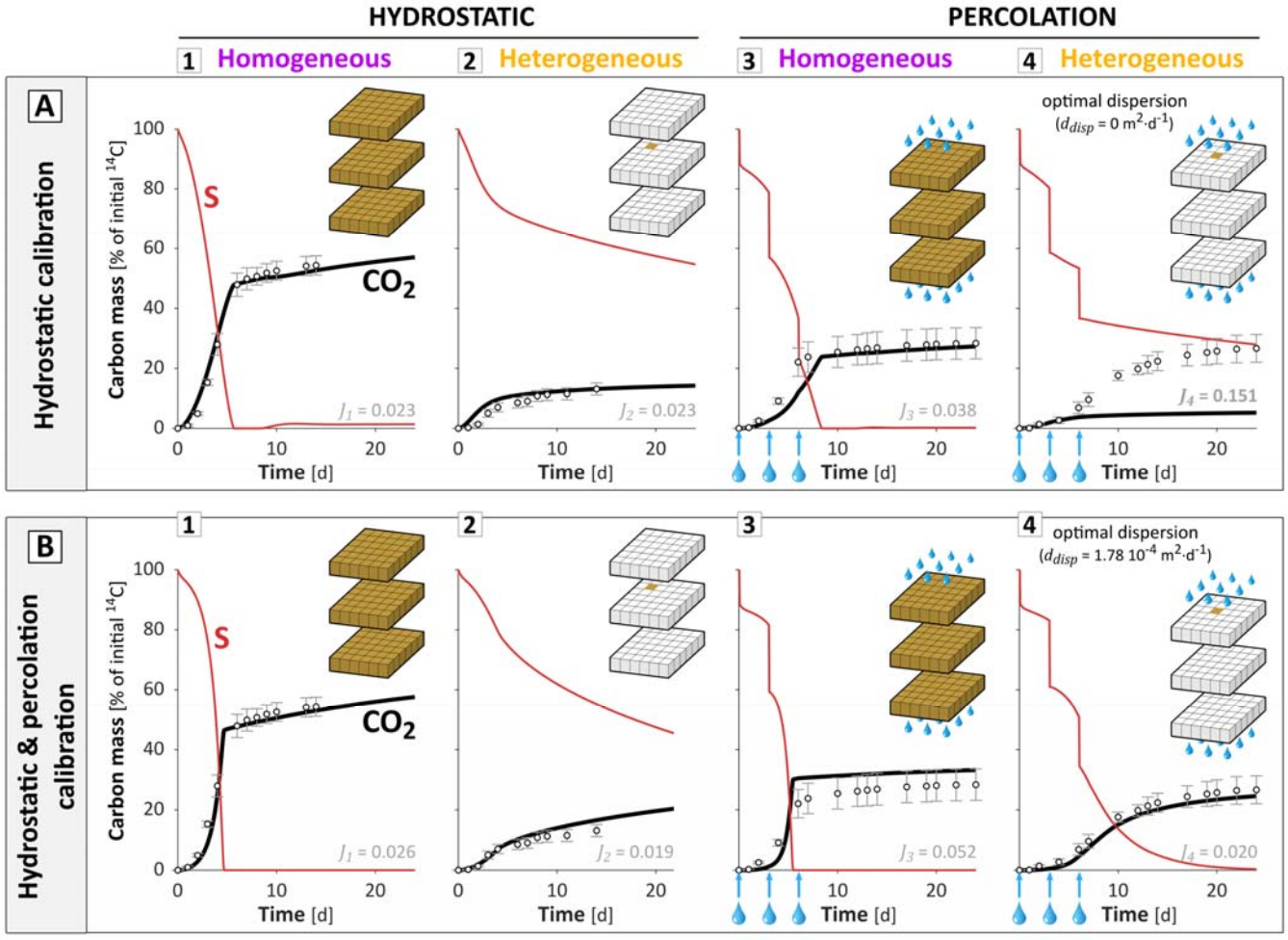

Fig. 3. Mineralization dynamics predicted with the Monod-based model calibrated on the hydrostatic experiment only (**A**) and on both hydrostatic and percolation experiments (**B**). The related experimental setups are indicated in the top right corner of each graph. The agreement between experiments and model is indicated by the value of discrepancy *J* displayed on top and can be visually assessed by the proximity between the black line and the dots representing respectively the model results and experimental data. The red line refers to the carbon mass of substrate remaining in the soil core. In the percolation experiments (**A3,4** and **B3,4**), around 51% of the initial mass of ^{14}C was lost through leaching at each

315 percolation events (t = 0, 3 and 6 days, blue arrows). The carbon balance among the different pools is
316 detailed in **Fig. S7**. Note that the reversible sorption eventually accounted for less than 2% of the initial
317 carbon mass and therefore did not significantly alter the results.

318 *3.2. Analysis of the controls exerted on degradation by substrate dilution and bacterial*
319 *density*

320 The effect of dispersion on degradation differed greatly between the two calibrated sets of biological
321 parameters described in section 3.1. We therefore conducted a more systematic investigation of the
322 coupled impact of bacterial dispersion and bacterial traits on degradation, revealing its control by substrate
323 dilution and bacterial density.

324 *3.2.1 Impact of dispersion on degradation*

325 We used the mineralization at the end of the experimental time (day 24) as a proxy for degradation and
326 determined its sensitivity to dispersion, as a function of the parameterization of bacterial traits. **Fig. 4**
327 shows the impact of the dispersion coefficient d_{disp} on the final predicted mineralization for the two
328 calibrated biological parameter sets, all other parameters being kept constant (thick red and blue lines). For
329 the biological parameter set calibrated on hydrostatic experiments, the final mineralization decreased
330 monotonically with dispersion (**Fig. 4**, red line). For the parameter set calibrated on both hydrostatic and
331 percolation experiments, the final mineralization first increased, reached a maximum around
332 $d_{disp} \approx 10^{-4}$ m^2·d^{-1} and then decreased (**Fig. 4**, blue line). These two kinds of behaviors were observed
333 regardless of the parameters α, $(1/y)\cdot\mu_{max}$ and $B(t=0)$ as long as $(1/y)\cdot\mu_{max}/\kappa_M$ remained the same
334 (**Fig. S8**). The non-monotonic impact of dispersion on degradation highlights the existence of an optimal
335 bacterial dispersion for which mineralization is the highest. The comparison between the red and blue lines
336 on **Fig. 4** suggests that the optimal dispersion value depends on the bacterial uptake efficiency. Note that,

337 although the optimal dispersion value varied with time due to the spatial dynamics of both bacteria and
338 substrate (**Fig. S9**), it tended towards a limit that was mostly reached within 4 to 7 days and is thus
339 represented at day 24 on **Fig. 4**.

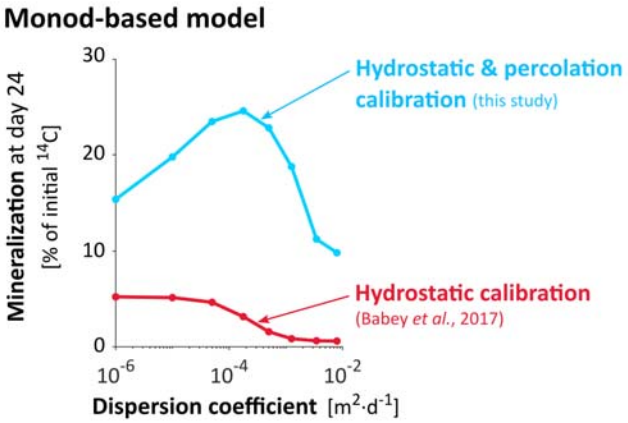

340

341 **Fig. 4.** Influence of the dispersion coefficient d_{disp} on mineralization predicted at day 24 $m_{CO2}(t=24)$ for the
342 biological parameter set calibrated on the sole hydrostatic experiments (**A**, thick red line) and on both
343 hydrostatic and percolation experiments (**B**, thick blue line). Note that for the model calibrated on both
344 hydrostatic and percolation experiments, the value of d_{disp} leading to the highest final mineralization
345 (d_{disp} = 1.78 10^{-4} $m^2 \cdot d^{-1}$, thick blue line) is also equal to its calibrated value leading to the best adequacy with
346 mineralization kinetics (**Table 2**).

347 *3.2.2 Double control of degradation by substrate dilution and bacterial density*

348 The non-monotonic effect of bacterial dispersion on degradation is an unusual and key feature of the
349 model calibrated on both hydrostatic and percolation experiments. In the following we will present an
350 explanation for how such relationships between dispersion and degradation could arise, resulting from a
351 non-monotonic spatial substrate profile, itself derived from the respective effects of substrate dilution and
352 bacterial density.

353 In the model, the instant exposure of bacteria to their substrate is maximal if all the bacteria are located
354 inside the voxel(s) with the highest substrate concentration. In the hydrostatic calibrated parameter set,
355 the profile of substrate concentration primarily resulted from its initial heterogeneity (bell-shape red curve
356 on **Fig. 5A** and pseudo bell-shape red curve on **Fig. 5B**). The flux of substrate reaching each bacterium was
357 therefore mostly determined by the distance between the bacterium and the initial location of substrate.
358 The exposure of a single bacterium to the substrate decreased with its distance from the substrate initial
359 location. This effect is referred to as "substrate dilution". In these cases (**Fig. 5A** and **B**), mineralization was
360 mainly regulated by substrate dilution, and therefore reduced by bacterial dispersion (**Fig. 4**, blue line).
361 However, for the parameter set calibrated on both hydrostatic and percolation experiments, local
362 degradation by aggregated bacteria reshaped the substrate spatial profile, thus critically changing the
363 voxel(s) with the highest substrate concentration. The bacteria aggregated at their initial location
364 consumed the substrate much faster than it was replenished by backward diffusion and dispersion,
365 creating a critical inversion of the substrate gradient, which led to an intra-population competition for
366 substrate (**Fig. 5C**). The competition was critical for bacterial densities as small as 3.5 10^{-3} $g{\cdot}l^{-1}$ (**Fig. 5C**). In
367 contrast, the dispersion of bacteria reduced competition by diluting the highest bacterial densities, thus
368 flattening the substrate gradient inversion induced by bacterial local degradation, resulting in a better
369 overall exposure of bacteria to the substrate concentrations, and thus an enhanced mineralization
370 (**Fig. 5D**). In these cases (**Fig. 5C** and **D**), mineralization was mainly regulated by bacterial density. This
371 relation between the bacterial density and the limitation of their exposure to the substrate is not
372 instantaneous and is mediated by the substrate concentration. This is expressed in the model equations
373 through the dependence of bacterial activity $\mu(t)$ on substrate concentration $S(t)$ (Eq. (7)) and the
374 dependence of the substrate concentration $S(t)$ on degradation $\mu(t){\cdot}B(t)$ (Eq. (1)), within each voxel.
375 However, when bacterial dispersion was too great, substrate dilution became the dominant control again.
376 This suggests that an optimal bacterial spatial spread exists for which the dilution of substrate is

377 compensated by the dilution of high local bacterial densities. The modeled scenario illustrated by the two
378 calibrated parameter sets were also observed for most of the other parameter sets. The optimal dispersion
379 coefficient for the 300 best-fitting parameterizations to both hydrostatic and percolation experiments
380 (smallest J_{1234} values) was on average $d_{disp} \approx 2\ 10^{-5}$ m^2·d^{-1} (**Fig. S10**), corresponding to a root-mean-square
381 displacement of bacteria of 1.5 to 3.5 mm during each percolation event.

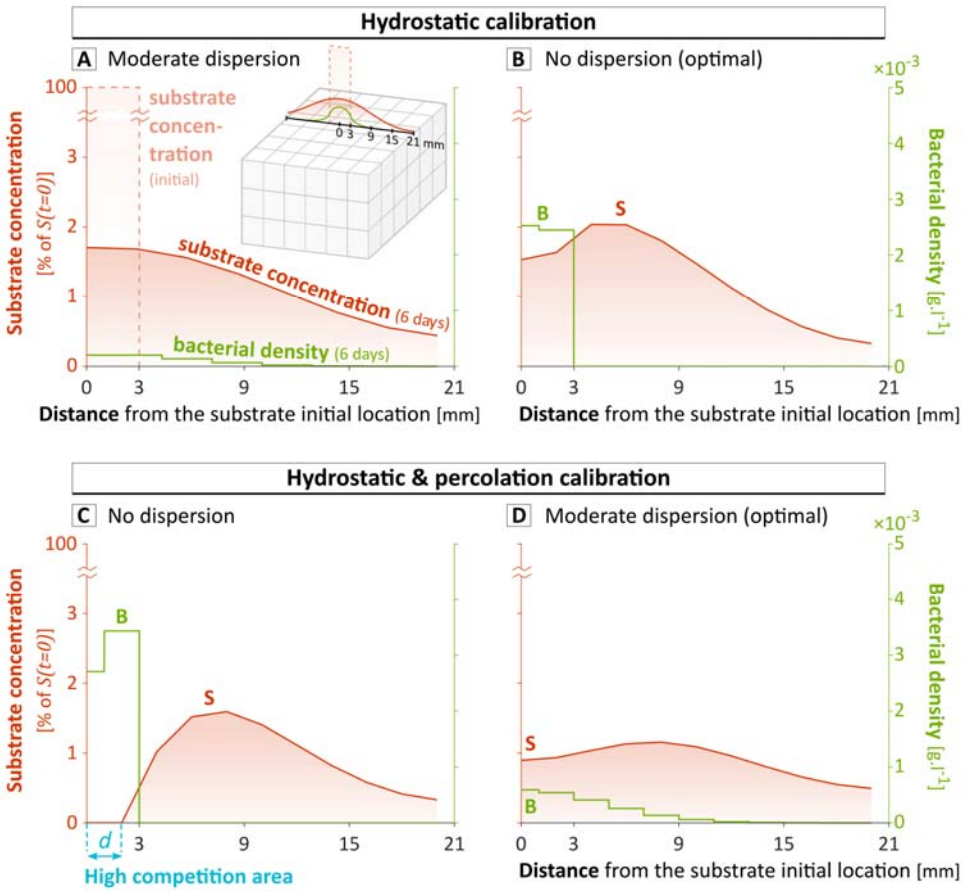

382

Fig. 5. Predicted substrate and bacterial spatial concentration profiles after6 days of diffusion and
384 dispersion in the conditions of heterogeneous percolation experiment, in which bacteria and substrate are
385 initially located exclusively in the central cube (between 0 and 3 mm). Results are simulated on a
386 9 × 18 × 18 grid obtained by subdividing the 3 × 6 × 6 grid used for the screenings. The results are
387 represented for the parameter set calibrated using only the sole hydrostatic experiment, either with a
388 moderate dispersion (d_{disp} = 1.78 10^{-4} m^2·d^{-1}) (**A**) or with the calibrated dispersion (no dispersion) (**B**), and

389 for the biological parameter set calibrated on both hydrostatic and percolation experiments, either without
390 dispersion (**C**) or with the calibrated dispersion (d_{disp} = 1.78 10^{-4} $m^2 \cdot d^{-1}$) (**D**). On one hand, bacteria are
391 exposed to smaller substrate concentrations if they are far from the source (right part of the substrate
392 concentration profiles). On the other hand, bacteria undergo competition if they are too close from each
393 other (left part of the substrate concentration profiles). In (**C**), the bacteria aggregated below d consume
394 the substrate faster than it is replenished by backward diffusion and dispersion. The total number of
395 bacteria within the whole soil column at day 6 is similar in (**A**), (**B**), (**C**) and (**D**), respectively equal to 6.0 10^5,
396 9.5 10^5, 11.5 10^5 and 11.3 10^5. The final mineralization at day 24 is however strongly different between
397 scenario, reaching respectively 3.2%, 5.3%, 9.1% and 24.7% of the initial mass of ^{14}C.

398 *3.2.3 Effect of bacterial uptake efficiency on the impact of dispersion on degradation*

399 A non-monotonic substrate concentration profile only occurs when bacterial degradation locally depletes
400 the substrate faster than it is replenished by diffusion. This area of high local competition for substrate
401 results from either high local densities of bacteria or high competitiveness or both. Bacterial
402 competitiveness is related to their maximum uptake efficiency $(1/y) \cdot \mu_{max}/\kappa_M$, which also describes their
403 capacity to maintain their activity and growth under dilute substrate concentrations (Healey, 1980; Button,
404 1991; Lobry et al., 1992). Bacteria with high maximum uptake efficiency are thus expected to benefit more
405 from dispersion. **Fig. 6** shows the optimal dispersion coefficient as a function of the maximum uptake
406 efficiency, with all other parameters equal to those of the model calibrated on both hydrostatic and
407 percolation experiments. The optimal dispersion coefficient, defined as the dispersion coefficient
408 maximizing the final mineralization, increased with the maximum uptake efficiency. For small maximum
409 uptake efficiencies of 30 $l \cdot g^{-1} \cdot d^{-1}$ and below, mineralization was highest in the absence of dispersion,
410 suggesting a regulation dominated by substrate dilution. For larger maximum uptake efficiencies,
411 dispersion impacted positively mineralization, suggesting that degradation shifted from being regulated by

substrate dilution to being regulated by bacterial densities, as bacteria were both more prone to competition between themselves and more efficient under diluted substrate conditions. In other words, the proximity to other bacteria constrained activity more than the proximity to the substrate initial location enhanced it. This combined effect of the maximum uptake efficiency and the bacterial dispersion on degradation was a general relationship common to all parameterizations (**Fig. S11**).

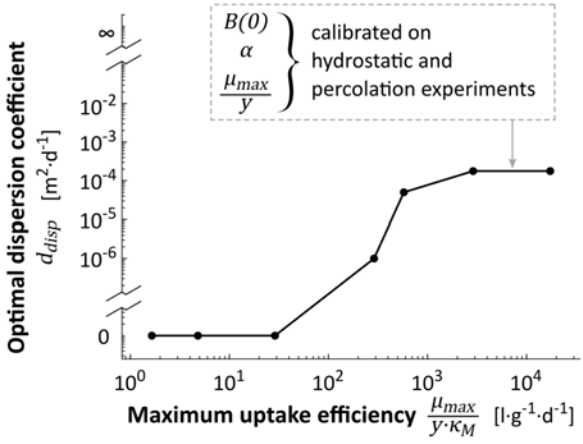

Fig. 6. Dispersion coefficient giving the highest predicted mineralization at day 24 as a function of maximum uptake efficiency, all other parameters equal to those of the model calibrated on both hydrostatic and percolation experiments.

3.3. The Contois-based model as an alternative to Monod

Given that degradation is regulated by both substrate dilution and bacterial density, and that their relative importance is modulated by bacterial uptake efficiency at the lowest substrate concentration, $(1/y)\cdot\mu_{max}/\kappa_M$, we investigated the relevance of the Contois model by applying the calibration methodology of section 2.4, as used in section 3.1. The interest in the Contois growth law (Eq. (8)) stems from the inclusion of a regulation by density in the expression of the uptake efficiency at the lowest substrate concentration, becoming $(1/y)\cdot\mu_{max}/(B(t)\cdot\kappa_C)$.

In comparison with the Monod-based model, the predictions of the experimental observations of Pinheiro et al. (2015, 2019) were facilitated with the Contois-based model, on three levels. First, the Contois-based model captured the degradation dynamics better than the Monod-based model, especially for the 1% best-fitting parameterizations (smallest J_{1234} values) (**Fig. S12**). The calibrated Contois-based model had an overall discrepancy of $J_{1234} = 0.022$ (**Fig. 7**), which was smaller than the lowest value of $J_{1234} = 0.032$ obtained for the calibrated Monod-based model (**Fig. 3**).

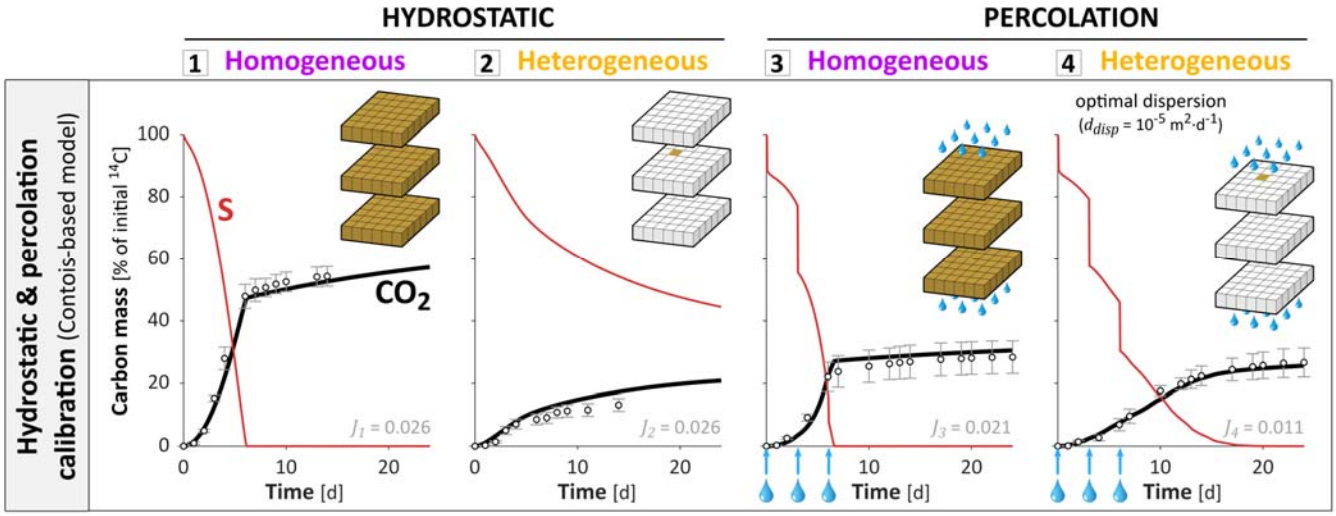

Fig. 7. Mineralization dynamics predicted with the Contois-based model calibrated on both hydrostatic and percolation experiments. For representation and legend, see **Fig. 3**. The carbon balance among the different pools is detailed in **Fig. S7**.

Second, the parameter sets that fitted homogeneous experiments also performed well under heterogeneous conditions, as long as the dispersion coefficient d_{disp} was calibrated as well (**Fig. S13**). It is an important advantage as it confers a better capacity to predict degradation kinetics for heterogeneous and varying distributions, once the model is calibrated in homogeneous conditions, which are more appropriate for the experimental measurement of bacterial parameters. Besides, using a dispersion coefficient value different from the calibrated one weakened the predictions of the mineralization dynamics but not the predictions of the mineralization after 24 days, which remained satisfying regardless of the dispersion coefficient. More precisely, the prediction of the final mineralization became mostly independent of the dispersion coefficient, as shown for the calibrated model (**Fig. 8**). This is because, in the Contois model at low substrate concentrations, the number of active bacteria in a soil volume is exactly counterbalanced by the regulation of their uptake efficiency by population density (Eq. (8)), resulting in limited effects of bacterial spreading on overall mineralization (**Fig. 8**, constant part of the curves).

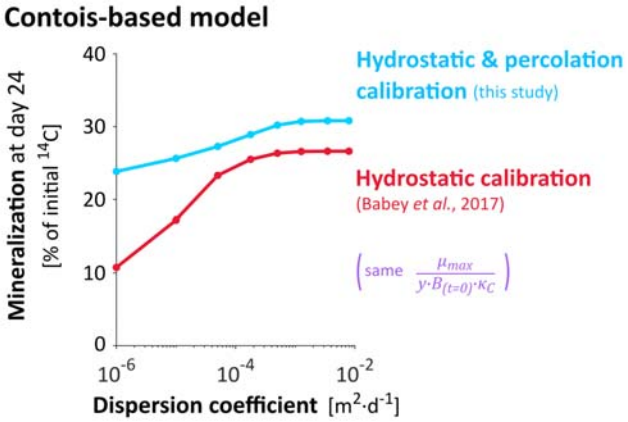

Fig. 8. Influence of the dispersion coefficient on mineralization at day 24 for the Contois-based models calibrated on the sole hydrostatic experiments (thick red line) and on both hydrostatic and percolation experiments (thick blue line). For representation and legend, see **Fig. 4**.

4. Discussion

4.1. Relevance of density control for 2,4-D degradation and soil carbon cycling

4.1.1 Density control of soil oligotroph bacteria

Bulk soil and highly-diluted environments are usually found to be dominated by bacteria with high maximum uptake efficiency, also called oligotrophs (Fierer et al., 2007; Nunan et al., 2020). Their high maximum uptake efficiency differentiates their life-history strategies and conditions their ability to thrive in resource poor environments (Button, 1993), also assimilated to K-strategy (Tecon and Or, 2017), by opposition to copiotrophic bacteria adapted to rich environments (r-strategy). The maximum uptake efficiency values of the 1% best-fitting parameter sets were of the order of 10^{3}-10^{4} $l \cdot g^{-1} \cdot d^{-1}$ (volume of water per mass of bacteria per unit of time), within the range proposed by Button (1991) to define oligotrophs. Similar or higher maximum uptake efficiency values of the order of 10^{4}-10^{5} $l \cdot g^{-1} \cdot d^{-1}$ have been reported for soil oligotrophs (Ohta and Taniguchi, 1988; Zelenev et al., 2005). Values up to 1.64 10^{5} have been reported by Tuxen et al. (2002) for 2,4-D degraders in an aerobic aquifer and even greater values might also be possible (see section S5). The high maximum uptake efficiencies predicted in section 3.1 for the best-fitting parameterizations are therefore a plausible bacterial trait among 2,4-D degraders as well as bulk soil bacteria in general. It suggests that density control might be relevant for a component of soil bacteria, which would benefit from dispersion as suggested by **Fig. 6**. The calibrated model has shown in section 3.2.2 that the values of densities from which competition became critical were around 3.5 10^{-3} $g \cdot l^{-1}$, corresponding to 7.5 10^{-7} $g \cdot g$ (mass of bacteria per mass of dry soil), ranging in the low end of usual total

soil bacterial densities (Raynaud and Nunan, 2014; Kuzyakov and Blagodatskaya, 2015). This suggests that competition might play a significant role even under the low bacterial densities observed in bulk soils. Reciprocally, the model suggests that competition for substrate between copiotrophic bacteria only appears at much larger population densities, such as those found in soil biofilms (Holden et al., 1997, Or et al., 2007). Interestingly, copiotrophic bacteria have been reported to cohabit with oligotrophic bacteria even in diluted environments (Gözdereliler et al., 2012). Results from the screening suggest that, for densities of copiotrophs as low as for oligotrophs, their impact on overall decomposition in dilution-dominated environments would be much lower due to their poorly adapted uptake efficiency (**Fig. 4A**). Conversely, this striking density regulation might be one of the main limitations of the overall population densities in soils. Note that this density regulation occurs within a single population with homogeneous biological constants. Spatial heterogeneities and low substrate concentrations, common in bulk soil, may indeed shift competition from the inter-population level to the intra-population level (Pfeiffer et al., 2001; Roller and Schmidt, 2015).

4.1.2 A new perspective on Regulatory Gate hypothesis

Density regulation might partially contribute to explain the common paradox of the apparent uncoupling between the overall mineralization of a soil volume and the size of its microbial population (Kemmitt et al., 2008). The rate of soil carbon mineralization remains the same even if 90% of the microbial decomposers are killed. This observation is commonly explained by the Regulatory Gate hypothesis, where mineralization is assumed to be controlled by an abiotic process, such as desorption or diffusion, that limits the availability of the substrate, resulting in mineralization rates that are independent of the degrader abundance. We propose that the density regulation of decomposition in oligotrophic environments may contribute to this phenomenon, through competition for substrate or other biological interactions. In the case of competition-related density regulation, it reduces the dependence of the overall carbon mineralization on degrader abundance, as any increase of population density counterbalances the effect of

497 the increased population size. Note that the involved abiotic process, namely the substrate diffusion
498 backward to bacteria (see section 3.2), is well limiting but only in situations of high bacterial competition.

499 *4.2. Relevance of the ratio-dependent Contois model in soils*

500 As argued in section 3.3, ratio-dependence might facilitate decomposition modeling in the soil conditions
501 typical of the experiments analyzed here. The Contois model's $(1/y)\cdot\mu_{max}/\kappa_C B$ calibrated in homogeneous
502 conditions might be used in heterogeneous conditions more reliably than the Monod model's
503 $(1/y)\cdot\mu_{max}/\kappa_M$, at least for soil systems in which the competition for the substrate plays a substantial role
504 within the degrader population. The similarity between κ_M and $\kappa_C B$ suggests the need to consider
505 population density when measuring the apparent maximum uptake efficiency of soil bacteria to avoid
506 underestimating it by unintentionally including density regulation. Moreover, the better predictions
507 obtained with the Contois model in the soil conditions represented by the experiments suggest that the
508 Contois ratio-dependence includes not only the effect of competition for substrate at the scale of
509 measurement, but it can also reasonably reflect other density processes such as the spatial variability of
510 bacterial distributions at finer scales related to their high degree of local aggregation in microcolonies
511 (Raynaud and Nunan, 2014). Moreover, ratio-dependence may also include the cumulative effects of
512 ecological interactions other than competition (Sibly and Hone, 2002). Note that the methodological
513 approach used in this study for both Monod and Contois models is based on an effective representation of
514 concentrations and parameters at the mm- to cm-scale of measurements. These effective concentrations
515 and parameters conceptually integrate the smaller-scale processes highlighted by other studies (Ebrahimi
516 and Or, 2014; Portell et al., 2018; Tecon et al., 2018). Such microscale processes should be addressed for
517 further generalization beyond the conditions of the soil experiments analyzed here. Despite its advantages,
518 Contois models have also a drawback with the fact that the modeled uptake efficiency of bacteria
519 approaches infinity for low densities, which does not correspond to any physical nor biochemical process

(Gleeson, 1994; Abrams, 2015). However, this side effect mostly affects a negligible fraction of the bacteria and the substrate, as it was the case in the soil conditions represented by the experiments.

Further work is required to confront the relevance of the Contois model to other soil systems. To the best of our knowledge, ratio-dependent growth models such as the Contois model have not yet been considered for the modeling of microbial degradation in soils. However, the Contois growth equation is generally accepted to be more appropriate than the Monod equation for modeling immobilized, heterogeneously distributed or mixed microbial cultures (Arditi and Saiah, 1992; Harmand and Godon, 2007), all of which are characteristics of soils. The regulation of individual activity by population density has frequently been justified as a "crowding effect" associated with high population densities leading to competition for substrate (Lobry and Harmand, 2006; Harmand and Godon, 2007; Krichen et al., 2018). However, little is known about possible density regulation when apparent microbial densities are low, as is observed in bulk soil (Raynaud and Nunan, 2014; Kuzyakov and Blagodatskaya, 2015), although some studies have mentioned ratio-dependence in highly-diluted environments such as aquifers (Hansen et al., 2017). As discussed in section 4.1.1, the high maximum uptake efficiencies commonly observed for soil bacteria adapted to oligotrophic environments are relevant to draw attention on the potential significance of density control at low densities in oligotrophic soils, and thus ratio-dependent models, among which the Contois model is a consistent choice.

4.3. Hypothetical relationship between bacterial traits and their spatial strategies

Density regulation might be at the origin of a relationship between bacterial oligotrophy, their location in soil and their mobility strategy. Soil copiotroph bacteria have a maximum uptake efficiency mostly between 100 $l \cdot g^{-1} \cdot d^{-1}$ (Button, 1991) and 800 $l \cdot g^{-1} \cdot d^{-1}$ (Daugherty and Karel, 1994; Zelenev et al., 2005). For copiotrophs with maximum uptake efficiency values below 288 $l \cdot g^{-1} \cdot d^{-1}$, bacterial dispersion was largely detrimental to their activity (**Fig. 4** blue line, **Fig. 6**), in agreement with the results of Pagel et al. (2020),

543 suggesting that copiotrophs have more aggregated distributions than oligotrophs. The negligible
544 mineralization even without dispersion (**Fig. 3-A4**, **Fig. S8**) also highlights the fact that copiotrophs are
545 particularly inefficient at degrading substrates that diffuse in the environment, as also evidenced by Babey
546 et al. (2017). To maintain significant activity, soil copiotrophs are likely to remain immobile in the close
547 surroundings of the substrate source or any immobile substrate, likely attached to surfaces or embedded in
548 EPS matrices. If not, they would be dispersed towards more diluted area where their low maximum uptake
549 efficiency would result in negligible uptake. On the contrary, to survive and develop, soil oligotrophs should
550 be able to easily disperse and escape high competition areas. Given that soil is a poor and heterogeneous
551 environment, this dispersion would be essentially passive (Nunan et al., 2020), through advective processes
552 for example. We therefore suggest the existence of a theoretical relationship between proximity to
553 substrate sources (respectively remoteness), copiotrophy (respectively oligotrophy) and attachment
554 (respectively mobility).

555 5. Conclusions

556 Heterogeneous distributions of degraders and substrate in soils strongly control soil organic matter
557 degradation through their interactions with the bacterial activity. Taking 2,4-D as a model organic solute
558 substrate for soil bacteria, we investigated the coupled effects of bacteria and substrate distributions on
559 one side and bacterial traits on the other side on substrate degradation. The analysis of published
560 experiments with contrasted spreading conditions of both bacteria and substrate reveals that, in addition
561 to the distance of bacteria from high substrate concentrations, mineralization is also surprisingly limited by
562 the bacterial density even under the low bacterial densities commonly observed in bulk soils. Moreover,
563 the impact of bacterial dispersion on solute substrate degradation can shift from negative to positive
564 depending on the bacterial maximum uptake efficiency. The activity of soil oligotrophs may be mostly
565 regulated by bacterial density rather than by substrate dilution, echoing the population size paradox

regularly observed. It follows that the ratio-dependent Contois model might be more relevant to model bulk soil mineralization in the heterogeneous conditions investigated than the substrate-dependent Monod model. To predict the impact of spatial distributions on degradation in oligotrophic soil, and more particularly the impact of bacterial dispersion, we suggest that bacterial densities might be a more useful measurement than the volumes of soil devoid or occupied with bacteria. With respect to the current lack of direct microscale data on microbial processes and distributions, we propose some key perspectives on the bacterial kinetics and distributions.

Acknowledgements

This work was supported by the Agence Nationale de la Recherche through the project "Soilμ-3D" [grant number ANR-15-CE01-0006] and was also partially supported by the SLAC Floodplain Hydro-Biogeochemistry Science Focus Area (SFA), which is funded by the U.S. Department of Energy (DOE) office of Biological and Environmental Research (BER), Climate and Environmental Sciences Division, under DOE contract No. DE- AC02-76SF00515 to SLAC. The authors thank Jérôme Harmand, Théodore Bouchez, Xavier Raynaud, Tanguy Le Borgne, Claire Chenu and Holger Pagel for insightful discussions.

Appendix A. Supplementary data

References

Abbott, A.J., Nelsestuen, G.L., 1988. The collisional limit: an important consideration for membrane-associated enzymes and receptors. The FASEB Journal 2, 2858–2866. https://doi.org/10.1096/fasebj.2.13.2844615

585 Abrams, P.A., 2015. Why ratio dependence is (still) a bad model of predation: Ratio-dependent predation.
586 Biological Reviews 90, 794–814. https://doi.org/10.1111/brv.12134
587 Arditi, R., Saiah, H., 1992. Empirical evidence of the role of heterogeneity in ratio-dependent consumption.
588 Ecology 73, 1544–1551. https://doi.org/10.2307/1940007
589 Babey, T., Vieublé Gonod, L., Rapaport, A., Pinheiro, M., Garnier, P., de Dreuzy, J.-R., 2017. Spatiotemporal
590 simulations of 2,4-D pesticide degradation by microorganisms in 3D soil-core experiments.
591 Ecological Modelling 344, 48–61. https://doi.org/10.1016/j.ecolmodel.2016.11.006
592 Bælum, J., Henriksen, T., Hansen, H.C.B., Jacobsen, C.S., 2006. Degradation of 4-chloro-2-
593 methylphenoxyacetic acid in top- and subsoil is quantitatively linked to the class III tfdA gene.
594 Applied and Environmental Microbiology 72, 1476–1486. https://doi.org/10.1128/AEM.72.2.1476-
595 1486.2006
596 Bælum, J., Nicolaisen, M.H., Holben, W.E., Strobel, B.W., Sørensen, J., Jacobsen, C.S., 2008. Direct analysis
597 of tfdA gene expression by indigenous bacteria in phenoxy acid amended agricultural soil. The ISME
598 Journal 2, 677–687. https://doi.org/10.1038/ismej.2008.21
599 Balkwill, D.L., Leach, F.R., Wilson, J.T., McNabb, J.F., White, D.C., 1988. Equivalence of microbial biomass
600 measures based on membrane lipid and cell wall components, adenosine triphosphate, and direct
601 counts in subsurface aquifer sediments. Microbial Ecology 16, 73–84.
602 https://doi.org/10.1007/BF02097406
603 Boivin, A., Amellal, S., Schiavon, M., van Genuchten, M.Th., 2005. 2,4-dichlorophenoxyacetic acid (2,4-D)
604 sorption and degradation dynamics in three agricultural soils. Environmental Pollution 138, 92–99.
605 https://doi.org/10.1016/j.envpol.2005.02.016
606 Breitenbeck, G.A., Yang, H., Dunigan, E.P., 1988. Water-facilitated dispersal of inoculant Bradyrhizobium
607 japonicum in soils. Biology and Fertility of Soils 7, 58–62. https://doi.org/10.1007/BF00260733

Bünemann, E.K., Bongiorno, G., Bai, Z., Creamer, R.E., De Deyn, G., de Goede, R., Fleskens, L., Geissen, V., Kuyper, T.W., Mäder, P., Pulleman, M., Sukkel, W., van Groenigen, J.W., Brussaard, L., 2018. Soil quality – A critical review. Soil Biology and Biochemistry 120, 105–125. https://doi.org/10.1016/j.soilbio.2018.01.030

Button, D.K., 1978. On the theory of control of microbial growth kinetics by limiting nutrient concentrations. Deep Sea Research 25, 1163–1177. https://doi.org/10.1016/0146-6291(78)90011-5

Button, D.K., 1983. Differences between the kinetics of nutrient uptake by micro-organisms, growth and enzyme kinetics. Trends in Biochemical Sciences 8, 121–124. https://doi.org/10.1016/0968-0004(83)90232-3

Button, D.K., 1991. Biochemical basis for whole-cell uptake kinetics: specific affinity, oligotrophic capacity, and the meaning of the michaelis constant. Applied and Environmental Microbiology 57, 2033–2038.

Button, D.K., 1993. Nutrient-limited microbial growth kinetics: overview and recent advances. Antonie van Leeuwenhoek 63, 225–235. https://doi.org/10.1007/BF00871220

Carrayrou, J., Mosé, R., Behra, P., 2004. Operator-splitting procedures for reactive transport and comparison of mass balance errors. Journal of Contaminant Hydrology 68, 239–268. doi:10.1016/S0169-7722(03)00141-4

Cheyns, K., Mertens, J., Diels, J., Smolders, E., Springael, D., 2010. Monod kinetics rather than a first-order degradation model explains atrazine fate in soil mini-columns: Implications for pesticide fate modelling. Environmental Pollution 158, 1405–1411. https://doi.org/10.1016/j.envpol.2009.12.041

Contois, D.E., 1959. Kinetics of bacterial growth: relationship between population density and specific growth rate of continuous cultures. Journal of General Microbiology 21, 40–50. https://doi.org/10.1099/00221287-21-1-40

Daugherty, D.D., Karel, S.F., 1994. Degradation of 2,4-dichlorophenoxyacetic acid by Pseudomonas cepacia DBOl(pRO101) in a dual-substrate chemostat. Applied and Environmental Microbiology 60, 3261–3267.

Dechesne, A., Owsianiak, M., Bazire, A., Grundmann, G.L., Binning, P.J., Smets, B.F., 2010. Biodegradation in a partially saturated sand matrix: compounding effects of water content, bacterial spatial distribution, and motility. Environmental Science & Technology 44, 2386–2392. https://doi.org/10.1021/es902760y

Dechesne, A., Badawi, N., Aamand, J., Smets, B.F., 2014. Fine scale spatial variability of microbial pesticide degradation in soil: scales, controlling factors, and implications. Frontiers in Microbiology 5, 667. https://doi.org/10.3389/fmicb.2014.00667

Desmond-Le Quéméner, E., Bouchez, T., 2014. A thermodynamic theory of microbial growth. The ISME Journal 8, 1747–1751. doi:10.1038/ismej.2014.7

Don, R.H., Weightman, A.J., 1985. Transposon mutagenesis and cloning analysis of the pathways for degradation of 2,4-dichlorophenoxyacetic acid and 3-chlorobenzoate in Alcaligenes eutrophus JMP134(pJP4). Journal of Bacteriology 161, 85–90.

Ebrahimi, A.N., Or, D., 2014. Microbial dispersal in unsaturated porous media: Characteristics of motile bacterial cell motions in unsaturated angular pore networks. Water Resources Research 50, 7406–7429. doi:10.1002/2014WR015897

Fierer, N., Bradford, M.A., Jackson, R.B., 2007. Toward an ecological classification of soil bacteria. Ecology 88, 1354–1364. https://doi.org/10.1890/05-1839

Gleeson, S.K., 1994. Density dependence is better than ratio dependence. Ecology 75, 1834–1835. https://doi.org/10.2307/1939642

Gözdereliler, E., Boon, N., Aamand, J., De Roy, K., Granitsiotis, M.S., Albrechtsen, H.J., Sørensen, S.R., 2012. Comparing metabolic functionality, community structure and dynamics of herbicide-degrading communities. Applied and Environmental Microbiology.

Haegeman, B., Rapaport, A., 2008. How flocculation can explain coexistence in the chemostat. Journal of Biological Dynamics 2, 1–13. https://doi.org/10.1080/17513750801942537

Hammond, E.C., 1938. Biological effects of population density in lower organisms. The Quarterly Review of Biology 13, 421–438. http://www.jstor.org/stable/2808555

Hansen, S.K., Pandey, S., Karra, S., Vesselinov, V.V., 2017. CHROTRAN: A mathematical and computational model for in situ heavy metal remediation in heterogeneous aquifers. ArXiv:1703.01381 [q-Bio].

Harmand, J., Godon, J.J., 2007. Density-dependent kinetics models for a simple description of complex phenomena in macroscopic mass-balance modeling of bioreactors. Ecological Modelling 200, 393–402. https://doi.org/10.1016/j.ecolmodel.2006.08.012

Healey, F.P., 1980. Slope of the Monod equation as an indicator of advantage in nutrient competition. Microbial Ecology 5, 281–286. http://www.jstor.org/stable/4250586

Holden, P.A., Firestone, M.K., 1997. Soil microorganisms in soil cleanup: How can we improve our understanding? Journal of Environment Quality 26, 32–40. https://doi.org/10.2134/jeq1997.00472425002600010006x

Holden, P.A., Hunt, J.R., Firestone, M.K., 1997. Toluene diffusion and reaction in unsaturated Pseudomonas putida biofilms. BIOTECHNOLOGY AND BIOENGINEERING 56, 15.

Iserles, A., 2009. A first course in the numerical analysis of differential equations, Cambridge University Press. ed.

574 Juyal, A., Otten, W., Falconer, R., Hapca, S., Schmidt, H., Baveye, P.C., Eickhorst, T., 2019. Combination of
575 techniques to quantify the distribution of bacteria in their soil microhabitats at different spatial
576 scales. Geoderma 334, 165–174. https://doi.org/10.1016/j.geoderma.2018.07.031

577 Kemmitt, S.J., Lanyon, C.V., Waite, I.S., Wen, Q., Addiscott, T.M., Bird, N.R.A., O'Donnell, A.G., Brookes,
578 P.C., 2008. Mineralization of native soil organic matter is not regulated by the size, activity or
579 composition of the soil microbial biomass—a new perspective. Soil Biology and Biochemistry 40,
580 61–73. https://doi.org/10.1016/j.soilbio.2007.06.021

581 Koch, A.L., 1971. The adaptive responses of Escherichia coli to a feast and famine existence, in: Advances in
582 Microbial Physiology. Elsevier, pp. 147–217. https://doi.org/10.1016/S0065-2911(08)60069-7

583 König, S., Vogel, H.-J., Harms, H., Worrich, A., 2020. Physical, chemical and biological effects on soil
584 bacterial dynamics in microscale models. Frontiers in Ecology and Evolution 8, 53.
585 https://doi.org/10.3389/fevo.2020.00053

586 Krichen, E., Harmand, J., Torrijos, M., Godon, J.J., Bernet, N., Rapaport, A., 2018. High biomass density
587 promotes density-dependent microbial growth rate. Biochemical Engineering Journal 130, 66–75.
588 https://doi.org/10.1016/j.bej.2017.11.017

589 Kuzyakov, Y., Blagodatskaya, E., 2015. Microbial hotspots and hot moments in soil: Concept & review. Soil
590 Biology and Biochemistry 83, 184–199. https://doi.org/10.1016/j.soilbio.2015.01.025

591 Lagneau, V., van der Lee, J., 2010. Operator-splitting-based reactive transport models in strong feedback of
592 porosity change: The contribution of analytical solutions for accuracy validation and estimator
593 improvement. Journal of Contaminant Hydrology 112, 118–129. doi:10.1016/j.jconhyd.2009.11.005

594 Lobry, C., Harmand, J., 2006. A new hypothesis to explain the coexistence of n species in the presence of a
595 single resource. Comptes Rendus Biologies 329, 40–46. https://doi.org/10.1016/j.crvi.2005.10.004

Lobry, J.R., Flandrois, J.P., Carret, G., Pave, A., 1992. Monod's bacterial growth model revisited. Bulletin of Mathematical Biology 54, 117–122. https://doi.org/10.1007/BF02458623

Madsen, E.L., Alexander, M., 1982. Transport of Rhizobium and Pseudomonas through Soil. Soil Science Society of America Journal 46, 557–560. https://doi.org/10.2136/sssaj1982.03615995004600030023x

Monod, J., 1949. The growth of bacterial cultures. Annual Review of Microbiology 3, 371–394. https://doi.org/10.1146/annurev.mi.03.100149.002103

Nelson, M.I., Holder, A., 2009. A fundamental analysis of continuous flow bioreactor models governed by Contois kinetics. II. Reactor cascades. Chemical Engineering Journal 149, 406–416. https://doi.org/10.1016/j.cej.2009.01.028

Nunan, N., Young, I.M., Crawford, J.W., Ritz, K., 2007. Bacterial interactions at the microscale - Linking habitat to function in soil, in: Franklin, R., Mills, A. (Eds.), The Spatial Distribution of Microbes in the Environment. Springer, Dordrecht, pp. 61–85.

Nunan, N., Schmidt, H., Raynaud, X., 2020. The ecology of heterogeneity: soil bacterial communities and C dynamics. Philosophical Transactions of the Royal Society B: Biological Sciences 375, 20190249. https://doi.org/10.1098/rstb.2019.0249

Ohta, H., Taniguchi, S., 1988. Growth characteristics of the soil oligotrophic bacterium: Agromonas oligotrophica JCM 1494 on diluted nutrient broth. The Journal of General and Applied Microbiology 34, 349–353. https://doi.org/10.2323/jgam.34.349

Or, D., Smets, B.F., Wraith, J.M., Dechesne, A., Friedman, S.P., 2007. Physical constraints affecting bacterial habitats and activity in unsaturated porous media – a review. Advances in Water Resources 30, 1505–1527. doi:10.1016/j.advwatres.2006.05.025

718 Pagel, H., Kriesche, B., Uksa, M., Poll, C., Kandeler, E., Schmidt, V., Streck, T., 2020. Spatial control of carbon
719 dynamics in soil by microbial decomposer communities. Frontiers in Environmental Science 8, 2.
720 https://doi.org/10.3389/fenvs.2020.00002

721 Pallud, C., Dechesne, A., Gaudet, J.P., Debouzie, D., Grundmann, G.L., 2004. Modification of spatial
722 distribution of 2,4-dichlorophenoxyacetic acid degrader microhabitats during growth in soil
723 columns. Applied and Environmental Microbiology 70, 2709–2716.
724 https://doi.org/10.1128/AEM.70.5.2709-2716.2004

725 Patarinska, T., Dochain, D., Agathos, S.N., Ganovski, L., 2000. Modelling of continuous microbial cultivation
726 taking into account the memory effects. Bioprocess Engineering 22, 517–527.
727 https://doi.org/10.1007/s004499900095

728 Pfeiffer, T., Schuster, S., Bonhoeffer, S., 2001. Cooperation and Competition in the Evolution of ATP-
729 Producing Pathways 292, 5.

730 Pieper, D.H., Reineke, W., Engesser, K.-H., Knackmuss, H.-J., 1988. Metabolism of 2,4-
731 dichlorophenoxyacetic acid, 4-chloro-2-methylphenoxyacetic acid and 2-methylphenoxyacetic acid
732 by Alcaligenes eutrophus JMP 134. Archives of Microbiology 150, 95–102.
733 https://doi.org/10.1007/BF00409724

734 Pinheiro, M., Garnier, P., Beguet, J., Martin Laurent, F., Vieublé Gonod, L., 2015. The millimetre-scale
735 distribution of 2,4-D and its degraders drives the fate of 2,4-D at the soil core scale. Soil Biology and
736 Biochemistry 88, 90–100. https://doi.org/10.1016/j.soilbio.2015.05.008

737 Pinheiro, M., Pagel, H., Poll, C., Ditterich, F., Garnier, P., Streck, T., Kandeler, E., Vieublé Gonod, L., 2018.
738 Water flow drives small scale biogeography of pesticides and bacterial pesticide degraders - A
739 microcosm study using 2,4-D as a model compound. Soil Biology and Biochemistry 127, 137–147.
740 https://doi.org/10.1016/j.soilbio.2018.09.024

741 Poll, C., Ingwersen, J., Stemmer, M., Gerzabek, M.H., Kandeler, E., 2006. Mechanisms of solute transport
742 affect small-scale abundance and function of soil microorganisms in the detritusphere. European
743 Journal of Soil Science 57, 583–595. https://doi.org/10.1111/j.1365-2389.2006.00835.x

744 Portell, X., Pot, V., Garnier, P., Otten, W., Baveye, P.C., 2018. Microscale Heterogeneity of the Spatial
745 Distribution of Organic Matter Can Promote Bacterial Biodiversity in Soils: Insights From Computer
746 Simulations. Frontiers in Microbiology 9, 1583. doi:10.3389/fmicb.2018.01583

747 Rapaport, A., 2018. Properties of the chemostat model with aggregated biomass. European Journal of
748 Applied Mathematics 29, 972–990. https://doi.org/10.1017/S0956792518000141

749 Raynaud, X., Nunan, N., 2014. Spatial Ecology of Bacteria at the Microscale in Soil. PLoS ONE 9, e87217.
750 https://doi.org/10.1371/journal.pone.0087217

751 Read, C.P., 1951. The "Crowding Effect" in Tapeworm Infections. The Journal of Parasitology 37, 174–178.
752 https://doi.org/10.2307/3273449

753 Roller, B.R., Schmidt, T.M., 2015. The physiology and ecological implications of efficient growth. The ISME
754 Journal 9, 1481–1487. https://doi.org/10.1038/ismej.2014.235

755 Shampine, L.F., Reichelt, M.W., 1997. The MATLAB ODE Suite. SIAM Journal on Scientific Computing 18, 1–
756 22. https://doi.org/10.1137/S1064827594276424

757 Sibly, R.M., Hone, J., 2002. Population growth rate and its determinants: an overview. Philosophical
758 Transactions of the Royal Society of London. Series B: Biological Sciences 357, 1153–1170.
759 https://doi.org/10.1098/rstb.2002.1117

760 Sinton, G.L., Fan, L.T., Erickson, L.E., Lee, S.M., 1986. Biodegradation of 2,4-D and related xenobiotic
761 compounds. Enzyme and Microbial Technology 8, 395–403. https://doi.org/10.1016/0141-
762 0229(86)90145-6

763 Smoluchowski, M. v, 1918. Versuch einer mathematischen Theorie der Koagulationskinetik kolloider
764 Lösungen. Zeitschrift für Physikalische Chemie 92U, 129–168. https://doi.org/10.1515/zpch-1918-
765 9209

766 Tecon, R., Or, D., 2017. Biophysical processes supporting the diversity of microbial life in soil. FEMS
767 Microbiology Reviews 41, 599–623. https://doi.org/10.1093/femsre/fux039

768 Tecon, R., Ebrahimi, A., Kleyer, H., Erev Levi, S., Or, D., 2018. Cell-to-cell bacterial interactions promoted by
769 drier conditions on soil surfaces. Proceedings of the National Academy of Sciences 115, 9791–9796.
770 doi:10.1073/pnas.1808274115

771 Tuxen, N., de Lipthay, J.R., Albrechtsen, H.-J., Aamand, J., Bjerg, P.L., 2002. Effect of exposure history on
772 microbial herbicide degradation in an aerobic aquifer affected by a point source. Environmental
773 Science & Technology 36, 2205–2212. https://doi.org/10.1021/es0113549

774 Ugalde-Salas, P., Desmond-Le Quéméner, E., Harmand, J., Rapaport, A., Bouchez, T., 2020. Insights from
775 Microbial Transition State Theory on Monod's Affinity Constant. Scientific Reports 10, 5323.
776 doi:10.1038/s41598-020-62213-6

777 Vieublé Gonod, L., Chenu, C., Soulas, G., 2003. Spatial variability of 2,4-dichlorophenoxyacetic acid (2,4-D)
778 mineralisation potential at a millimetre scale in soil. Soil Biology and Biochemistry 35, 373–382.
779 https://doi.org/10.1016/S0038-0717(02)00287-0

780 Young, I.M., Crawford, J.W., Nunan, N., Otten, W., Spiers, A., 2008. Chapter 4 Microbial distribution in soils,
781 in: Advances in Agronomy. Elsevier, pp. 81–121. https://doi.org/10.1016/S0065-2113(08)00604-4

782 Zelenev, V.V., van Bruggen, A.H.C., Semenov, A.M., 2005. Modeling wave-like dynamics of oligotrophic and
783 copiotrophic bacteria along wheat roots in response to nutrient input from a growing root tip.
784 Ecological Modelling 188, 404–417. https://doi.org/10.1016/j.ecolmodel.2005.01.046

785 Appendix A. Supplementary Data